

Critical phenomena at the threshold of immediate merger in binary black hole systems: the extreme mass ratio case

Carsten Gundlach¹, Sarp Akcay^{1,2}, Leor Barack¹ and Alessandro Nagar²
¹*School of Mathematics, University of Southampton, Southampton SO17 1BJ, UK*
²*Institut des Hautes Etudes Scientifiques, 91440 Bures-sur-Yvette, France*
(Dated: 21 July 2012, revised 11 September 2012)

In numerical simulations of black hole binaries, Pretorius and Khurana [Class. Quant. Grav. **24**, S83 (2007)] have observed critical behaviour at the threshold between scattering and immediate merger. The number of orbits scales as $n \simeq -\gamma \ln |p - p_*|$ along any one-parameter family of initial data such that the threshold is at $p = p_*$. Hence they conjecture that in ultrarelativistic collisions almost all the kinetic energy can be converted into gravitational waves if the impact parameter is fine-tuned to the threshold. As a toy model for the binary, they consider the geodesic motion of a test particle in a Kerr black hole spacetime, where the unstable circular geodesics play the role of critical solutions, and calculate the critical exponent γ . Here, we incorporate radiation reaction into this model using the self-force approximation. The critical solution now evolves adiabatically along a sequence of unstable circular geodesic orbits under the effect of the self-force. We confirm that almost all the initial energy and angular momentum are radiated on the critical solution. Our calculation suggests that, even for infinite initial energy, this happens over a finite number of orbits given by $n_\infty \simeq 0.41/\eta$, where η is the (small) mass ratio. We derive expressions for the time spent on the critical solution, number of orbits and radiated energy as functions of the initial energy and impact parameter.

CONTENTS

References

17

I. Introduction	1
II. Dynamical systems ideas	2
III. Test particles on Schwarzschild spacetime	3
A. Equations of motion	3
B. Critical solution	5
C. Perturbations of the critical solution	5
IV. Critical solution in the self-force approximation	5
A. Qualitative discussion	5
B. Equations of motion	6
C. Adiabatic expansion	6
D. Self-force input	7
E. Integration of the critical solution	7
F. The ultrarelativistic approximation	8
G. Validity of the self-force and adiabatic approximations	9
V. Critical scaling in the self-force approximation	9
A. Perturbations of the critical solution	9
B. Dependence on the initial data	11
C. Critical exponents in the geodesic case	11
D. Generalised critical scaling in the radiation reaction case	12
VI. Conclusions	14
Acknowledgments	15
A. Numerical data	15
B. Perturbation modes of the critical solution in the ultrarelativistic limit	16

I. INTRODUCTION

Motivated by speculation about the formation of black holes in high-energy particle collisions, there has recently been interest in binary black hole mergers with large initial boosts; see [1] for a review. A critical surface in phase space separates initial data which lead to merger from data which scatter at first approach, thus defining a *threshold of immediate merger* in the space of initial data. (Note that “scatter at first approach” here includes data which merge at a subsequent approach.)

Pretorius and Khurana [2] have numerically evolved initial data near this threshold for equal mass, non-spinning black hole binaries. They find that generic smooth one-parameter families of initial data intersect the threshold once, consistent with it being a smooth hypersurface in phase space. Moreover, they find that the number n of orbits before either merger or flying apart increases with fine-tuning to the threshold, with n scaling approximately as

$$n \simeq -\gamma \ln |p - p_*| + \text{constant}, \quad (1)$$

where p is any *smooth* parameter along the family of initial data, and p_* its value at the threshold of immediate merger. The additive constant depends on the family and on how p is defined, but the dimensionless *critical exponent* γ is independent of the family (for the reasons reviewed in Sec. II). In [2], where initial data with relative boosts of around 0.22 are evolved, (1) is found to be a good fit for $1 \lesssim n \lesssim 4$ with $\gamma = 0.35 \pm 0.03$.

In this regime, a fraction of 1 to 1.5% of the rest mass is radiated per orbit [2]. While their initial data are rest

mass-dominated, Pretorius and Khurana speculate that in large-boost initial data fine-tuned to the critical impact parameter, most of the initial kinetic energy, and hence most of the total energy, can be turned into gravitational radiation over a large number of orbits. This is quite different from the situation for either large [3, 4] or small [5, 6] impact parameter. Hence in a particle physics context, there is a small cross section (corresponding to fine-tuned impact parameter) in which the gravitational wave energy emitted is much larger than in a generic collision.

In a subsequent paper using a different numerical code, Spherhake and collaborators [7] evolved initial data with boosts around 1.5 and 2.9. The critical exponent γ is estimated as 0.2, and the scaling law is observed for the range $0.5 \lesssim n \lesssim 1.5$. No data for critical scaling of the energy are given but in these more relativistic collisions, the fraction of total energy radiated is reported to be as high as 35% for the higher boost. Comparison with the results of [2] suggests that γ and the energy radiated depend on the initial boost (initial energy).

Pretorius and Khurana [2] note that what they observe in full numerical relativity is similar to “zoom-whirl” behaviour [8] in the timelike geodesics of test particles in a black-hole spacetime when the impact parameter is fine-tuned to its critical value, now characterising the threshold of immediate capture. Hence they propose equatorial orbits of a test particle on a Kerr spacetime (with mass and angular momentum set to the total mass and angular momentum of the binary) as a toy model for the equal mass binary. They point out that the critical solutions mediating this behaviour are the unstable circular orbits, and use this to calculate the critical exponent for this toy model. We obtain their results as a limiting case of ours in Sec. V C below.

The presence of critical phenomena suggests the existence of a critical solution defined by having a single growing perturbation mode and usually also characterised by a symmetry. Because energy is lost through gravitational radiation, the critical solution cannot be stationary, and because the black holes have rest mass it cannot be self-similar. We suggest that the critical solution is an unstable “as circular as possible” orbit that in the limit where one of the two objects becomes a test particle is indeed one of the unstable circular orbits considered by Pretorius and Khurana.

In this paper, we extend their analysis to binaries with large but finite mass ratio, and include radiation reaction in the self-force approximation. We restrict to the case where the large black hole is Schwarzschild, but our methods are in principle applicable to Kerr. This mathematical approach allows us to clarify the nature of the critical solution as adiabatically stationary and, based on this, compute the orbit and radiation as a function of the initial data.

In the large mass ratio regime, we confirm the conjecture of Pretorius and Khurana that almost all the kinetic energy of the binary (which in turn is almost all the

total energy for ultrarelativistic collisions) is radiated if the fine-tuning of the initial data is sufficiently good. We find, however, that the number of orbits remains finite as fine-tuning is improved, while (1) holds only for sufficiently small η and $|p - p_*|$.

We begin by reviewing the general mathematical ideas behind critical phenomena in dynamical systems language in Sec. II. For reference, and to establish notation, we review timelike geodesics in Schwarzschild spacetime in Sec. III. We construct the critical solution in the self-force approximation in Sec. IV, and in Sec. V we investigate its perturbations and from these we derive expressions for the the total number of orbits and total energy radiated as functions of the initial energy and impact parameter. Sec. VI summarises our results and gives an outlook on the comparable mass case.

Throughout the paper \simeq denotes equality up to sub-leading terms, and \sim equality up to subleading terms and an overall constant factor, and $:=$ denotes a definition.

II. DYNAMICAL SYSTEMS IDEAS

We briefly review *type I critical phenomena* and the calculation of the related critical exponent, in the language of abstract dynamical systems. Let ϕ represent a point in phase space. This could be either a vector of variables or a vector of fields at one moment of time. Let $\phi(t)$ be a trajectory in phase space that represents a solution. For the basic critical phenomena picture, we do not need to distinguish between field theories and finite-dimensional dynamical systems (and so do not write any x -dependence). This will later allow us to approximate a field theory (general relativity) by a finite-dimensional dissipative dynamical system (particle orbits with self-force).

Assume that at late times there are two qualitatively distinct outcomes, such as scattering and plunge in our system. There must then be a hypersurface in phase space separating these two basins of attraction, called the *critical surface*. As solution curves in phase space cannot intersect, the critical surface must be a dynamical system in its own right. Assume that the critical surface, considered as a dynamical system, has an attractor, called the *critical solution* ϕ_* . As ϕ_* is a fixed point (independent of t), its linear perturbations must be a sum of modes of the form $e^{\lambda_i t} \phi_i$, with ϕ_i also independent of t . As ϕ_* is an attractor within the critical hypersurface, which itself is a repeller, ϕ_* must have precisely one growing mode, pointing out of the critical surface, for some (real) $\lambda_0 > 0$ [9].

Consider a one-parameter family of initial data, with parameter p , such that this family intersects the critical surface at $p = p_*$. The evolution of the precisely critical initial data with p_* must lie in the critical surface and hence will find ϕ_* . Consider now initial data near the critical surface, with $p - p_*$ sufficiently small so that $\phi(t)$ passes close to ϕ_* during the evolution, and we can use

perturbation theory about ϕ_* . There is then a range of t where the decaying modes can be already neglected and the growing mode ϕ_0 is still small enough for perturbation theory to hold, leading to the approximation

$$\phi(t) \simeq \phi_* + C_1(p - p_*)e^{\lambda_0 t} \phi_0, \quad (2)$$

where C_1 is some constant that depends on the particular one-parameter family. Now define t_* by

$$\phi(t_*) \simeq \phi_* + C_2 \phi_0, \quad (3)$$

where C_2 is a fairly arbitrary constant, representing a reference deviation from the critical solution where it becomes apparent on which side of the critical surface the solution is going to end up. One then finds

$$t_* \simeq -\Gamma \ln |p - p_*| + C_3, \quad (4)$$

where C_3 depends on C_1 and C_2 , and $\Gamma = 1/\lambda_0$ is called the *critical exponent*.

Essentially the same picture holds if ϕ_* is not a fixed point but a limit cycle (periodic in t). Then ϕ_0 is also periodic in t and so is C_3 , and this leads to a modulation of the scaling law periodic in $\ln |p - p_*|$. This generalisation is not relevant for our application, but might be for extreme-mass ratio orbits in Kerr not in the equatorial plane, or more generally for binaries with spin.

However, another generalisation is relevant here. As we shall see, in the geodesic toy model of Pretorius and Khurana the critical solution is not an isolated attractor, but instead there is a line of critical solutions (each of which represents an unstable circular orbit, and has precisely one growing mode). In the self-force approximation to extreme mass ratio binaries, by contrast, these merge into a single critical solution, which can be approximated as an adiabatic motion along the line of unstable circular geodesic orbits, and so is slowly time-dependent. The general dynamical system picture above remains again basically unchanged, except that in the first case ϕ_* , ϕ_0 and λ_0 form a one-parameter family (parameterised for example by the energy of the orbit), and in the second case they become slowly varying functions of t .

III. TEST PARTICLES ON SCHWARZSCHILD SPACETIME

A. Equations of motion

To establish notation, we review the trajectories of test particles, modelled as geodesics, on Schwarzschild spacetime. Let t, r, θ, φ be the usual Schwarzschild coordinates, so that the Schwarzschild metric is

$$ds^2 = -\left(1 - \frac{2}{r}\right) dt^2 + \left(1 - \frac{2}{r}\right)^{-1} dr^2 + r^2(d\theta^2 + \sin^2\theta d\varphi^2), \quad (5)$$

and let a dot denote the derivative with respect to the proper time τ of the particle. Throughout this paper we use units such that Newton's constant G , the speed of light c and the mass M of the Schwarzschild spacetime are all unity. Let $u^a = \dot{x}^a = dx^a/d\tau$ be the 4-velocity of the particle. Without loss of generality let the orbit be in the plane $\theta = \pi/2$. Define

$$E := -\left(\frac{\partial}{\partial t}\right)^a u_a, \quad (6)$$

$$L := \left(\frac{\partial}{\partial \varphi}\right)^a u_a, \quad (7)$$

representing the energy and angular momentum *per rest mass* of the test particle. Retaining the convention $c = G = 1$, but restoring M , and with m the mass of the test particle, its physical energy and angular momentum are mE and mML . As $\partial/\partial t$ and $\partial/\partial \varphi$ are Killing vectors of the Schwarzschild spacetime, E and L are conserved quantities in the sense that

$$\dot{E} = 0, \quad (8)$$

$$\dot{L} = 0 \quad (9)$$

along geodesic orbits. Hence we obtain

$$\dot{t} = \left(1 - \frac{2}{r}\right)^{-1} E, \quad (10)$$

$$\dot{\varphi} = \frac{L}{r^2}. \quad (11)$$

By definition, $E > 0$ for any timelike geodesic for $r > 2$, where $\partial/\partial t$ is future timelike. Without loss of generality we shall also assume $L \geq 0$. The normalisation condition $u_a u^a = -1$ can then be expressed as

$$E^2 = \dot{r}^2 + V(L, r), \quad (12)$$

where

$$V(L, r) := \left(1 - \frac{2}{r}\right) \left(1 + \frac{L^2}{r^2}\right). \quad (13)$$

Geodesics on Schwarzschild obey

$$u^b \nabla_b u^a = \ddot{x}^a + \Gamma^a_{bc} \dot{x}^b \dot{x}^c = 0, \quad (14)$$

but (8,9) together with the normalisation condition (12) can be used to reduce this 6-dimensional dynamical system to a 3-dimensional one in the variables (r, \dot{r}, L) , with the equations of motion

$$\ddot{r} = -\frac{1}{2} V_{,r}(L, r), \quad (15)$$

$$\dot{L} = 0, \quad (16)$$

and where $E(r, \dot{r}, L)$ defined by (12) is an integral of the motion. (Here and in the following, commas denote partial derivatives.) Alternatively, as long as \dot{r} does not

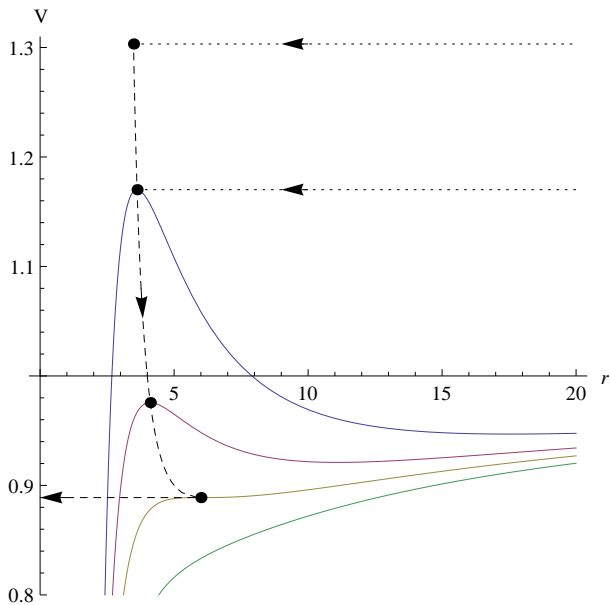


FIG. 1. **For Sec. III A:** Illustration of the effective potential (13) for different values of L . From above, the four full lines illustrate the cases $L > 4$, $\sqrt{12} < L < 4$, $L = \sqrt{12}$ and $L < \sqrt{12}$. Note that all these curves approach $V \rightarrow 1$ as $r \rightarrow \infty$. — **For Sec. IV A:** The dashed line represents the critical solution. Its almost vertical segment represents the adiabatic phase. As illustrated by the beads, it is given by $r(t) = r_-(L(t))$, $E^2(t) = V_-(L(t))$, with $\dot{L}(t)$ determined by radiation. The horizontal segment represents the plunge phase. The two dotted lines represent orbits coming in from infinity at the critical impact parameter for different E , and asymptoting to the critical solution. Radiation reaction has been neglected in the approach and plunge phases, while \dot{r} has been approximated as zero in the adiabatic phase. With radiation reaction, to order η the approach and plunge phase curves bend slightly downwards, the adiabatic curve is slightly further to the right, and the kinks are slightly smoothed out. [The beads are the maxima of the potential for $L = 5, 4.6, 3.9, \sqrt{12}$, and the lowest curve (without a maximum) corresponds to $L = 3$.]

change sign, the system can be written in the variables (r, L, E) in the form

$$\dot{r} = \pm \sqrt{E^2 - V(L, r)}, \quad (17)$$

$$\dot{L} = 0, \quad (18)$$

$$\dot{E} = 0, \quad (19)$$

which now shows both integrals of the motion explicitly. In either case, the variables (t, φ) are evolved by (10,11) and play no dynamical role, while the remaining component of (14) is consistent with our assumption $\theta = 0$.

The shape of the effective potential $V(L, r)$ for different ranges of L is illustrated in Fig. 1. (The dashed and dotted curves should be ignored for now.) As $V(L, \infty) = 1$ for any L , orbits with $E \geq 1$ are unbound. For $L > \sqrt{12}$, the effective potential has a maximum at $r = r_-$

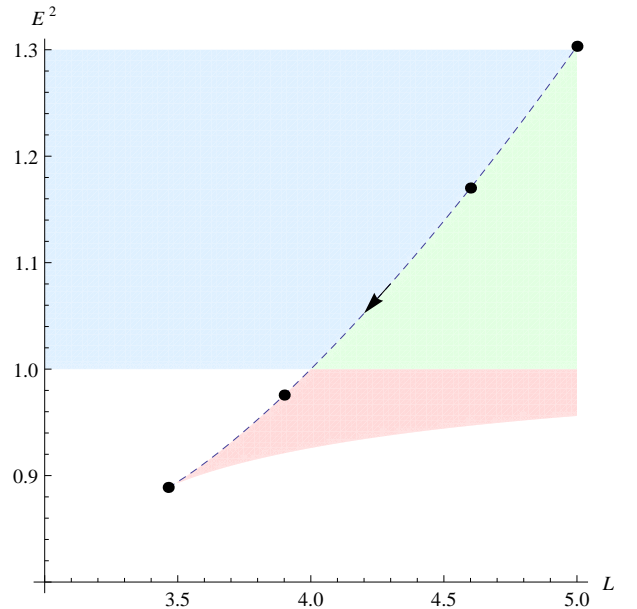


FIG. 2. **For Sec. III B:** The space of geodesics on Schwarzschild, labelled by angular momentum per unit mass L and energy per unit mass (squared) E^2 of the particle. The bottom right shaded region contains bound orbits that oscillate between a minimum and maximum radius. Its lower edge is given by stable circular orbits. The left shaded region contains orbits that come in from infinity with low impact parameter and plunge. The top right shaded region contains orbits that come in from infinity with high impact parameter and scatter. The line dividing these two regions is therefore the threshold of immediate capture, given by $E^2 = V_-(L)$ (which characterises unstable circular orbits). The white region corresponds to orbits that emerge from the white horizon and plunge back into the black hole, and which are not of interest to us here. — **For Sec. IV A:** In the self-force approximation, the critical solution moves adiabatically along the line of unstable circular geodesic orbits, as indicated by the dashed line and arrow. The beads and arrow are as in Fig. 1. (The approach and plunge phases seen in Fig. 1 are essentially in the r direction, which is suppressed here.)

and a minimum at $r = r_+$, given by

$$r_{\pm} := \frac{L(L \pm L_{12})}{2}, \quad (20)$$

where it takes values

$$V_{\pm} := V(r_{\pm}) = \frac{2(2L \pm L_{12})^2}{9L(L \pm L_{12})}. \quad (21)$$

Here we have introduced the shorthand

$$L_{12} := \sqrt{L^2 - 12}. \quad (22)$$

The minimum and maximum give rise to a stable and an unstable circular orbit. These merge for $L = \sqrt{12}$, at $r_+ = r_- = 6$.

For trajectories coming in from infinity, and hence with $E \geq 1$, a natural parameter of the initial data is the

impact parameter $b > 0$, defined by

$$b := \lim_{r \rightarrow \infty} r \sin |\varphi(r) - \varphi(\infty)|. \quad (23)$$

With

$$\frac{d\varphi}{dr} = \frac{L}{r^2 \sqrt{E^2 - V(L, r)}}, \quad (24)$$

we find

$$E^2 - 1 = \frac{L^2}{b^2}. \quad (25)$$

We define the (instantaneous) orbital angular frequency

$$\Omega := \frac{d\varphi}{dt} = \frac{\dot{\varphi}}{\dot{t}} = \left(1 - \frac{2}{r}\right) \frac{L}{r^2 E} = \frac{V_{,L}}{2E}. \quad (26)$$

For both the stable and unstable circular geodesic orbits, we have

$$E = \frac{r-2}{\sqrt{r(r-3)}}, \quad (27)$$

$$L = \frac{r}{\sqrt{r-3}}, \quad (28)$$

$$\Omega = r^{-3/2} \quad (29)$$

We will be particularly interested in the ultrarelativistic limit $E \gg 1$, where

$$E \simeq \frac{1}{\sqrt{3}}(r-3)^{-1/2}, \quad (30)$$

$$L \simeq 3(r-3)^{-1/2} \simeq 3\sqrt{3}E, \quad (31)$$

$$\Omega \simeq \frac{1}{3\sqrt{3}}. \quad (32)$$

B. Critical solution

For simplicity of presentation, in the following we discuss only geodesic orbits with $E > 1$ and which initially have $\dot{r} < 0$ and $r > r_-(L)$, coming in from large r . If the impact parameter is fine-tuned so that $E^2 = V_-(L)$, the orbit asymptotically approaches the unstable circular orbit $r = r_-(L)$, without ever plunging or moving back out. Orbits with the same L but smaller E scatter, while orbits with the same L but larger E plunge. Hence the critical surface in the space of initial data parameterised by (r, E, L) with $\dot{r} < 0$ is formed by the surface $E^2 = V_-(L)$, $r > r_-(L)$. The space of geodesic orbits is illustrated in Fig. 2.

We define the critical impact parameter $b_*(E)$ by $E^2 = V_-(L = L(E, b_*))$ and find

$$b_*(E) = \frac{\sqrt{27E^4 - 36E^2 + 8 + E(9E^2 - 8)^{3/2}}}{\sqrt{2}(E^2 - 1)}, \quad (33)$$

which has the well-known limits

$$b_*(\infty) = 3\sqrt{3} \quad (34)$$

and $b_*(1) = \infty$ (every particle released from rest at infinity falls into the black hole).

C. Perturbations of the critical solution

The linearisation of the dynamical system (15,16) about the critical solution $r = r_-(L)$ is

$$\delta\ddot{r} = -\frac{1}{2}V_{,rr-}\delta r - \frac{1}{2}V_{,rL-}\delta L, \quad (35)$$

$$\delta\dot{L} = 0, \quad (36)$$

where $V_{,rr-}$ and $V_{,rL-}$ are $V_{,rr}$ and $V_{,rL}$ evaluated on the critical solution $r = r_-(L)$. We can decouple these equations as

$$\ddot{x} = \Gamma^{-2}x, \quad (37)$$

$$\delta\dot{L} = 0, \quad (38)$$

where

$$x := \delta r + \frac{V_{,rL-}}{V_{,rr-}}\delta L, \quad (39)$$

$$\Gamma := \left(-\frac{1}{2}V_{,rr-}\right)^{-1/2} = \frac{L^{3/2}(L - L_{12})^2}{4L_{12}^{1/2}}. \quad (40)$$

With $E^2 = V_-(L)$ on the critical solution, we can consider Γ also as function of E , but we have not been able to express $\Gamma(E)$ in closed form.

From (35,36) we see that the critical solution has exponentially growing and decaying modes $x = \exp(\pm\tau/\Gamma)$ with $\delta L = 0$, and a neutral mode $\delta L = 1$ with $x = 0$. Hence it has precisely one growing mode, as required of a critical solution. However, in the geodesic approximation we do not have a critical solution which is a global attractor within the critical surface, but rather a line of critical solutions, to which the neutral mode is tangent.

IV. CRITICAL SOLUTION IN THE SELF-FORCE APPROXIMATION

A. Qualitative discussion

Our aim is to replace the model of the binary merger as a test particle on Schwarzschild spacetime with a more realistic model that in particular incorporates radiation reaction, but which still approximates the Einstein equations as a finite-dimensional dynamical system by integrating out the radiation.

One such model is the extreme mass-ratio approximation, where the loss of energy and angular momentum are calculated to leading order in $\eta := m/M$, where $M = 1$ is the mass of a large black hole and m that of the smaller object, modelled as a point particle. We shall use an adiabatic approximation, where the particle is considered to move on a geodesic with E and L now slowly decaying, and a force term appearing in consequence on the right-hand side of the geodesic equation. We can then still use the effective potential picture to write the equations of motion, where $E(t)$ and $L(t)$ now evolve under the effect of the radiation reaction.

In short, the critical solution sits approximately at the maximum of the potential, with $E(t)^2 = V_-(L(t)) + O(\eta)$ and $r(t) = r_-(L(t)) + O(\eta)$, while that maximum itself evolves under radiation reaction, starting with the ultra-relativistic limit (31) as $r \simeq 3$ and $E \rightarrow \infty$, and ending with a plunge from $E \simeq 8/9$, $L \simeq \sqrt{12}$ and $r \simeq 6$ (see Fig. 1). Our self-force calculation suggests that infinite E and L occur at *finite* τ , t and φ in the past, but as we discuss below, we cannot consistently reach $E = \infty$ within the self-force approximation.

Any initial data that are perfectly fine-tuned to the threshold of immediate merger, with arbitrarily large E , join the critical solution, which acts as an attractor in the critical surface. This is indicated schematically in Figs. 1 and 2, where the dotted lines with arrows indicate two fine-tuned solutions approaching the critical solution (dashed) and remaining on it until and through the plunge. Note that the line of critical fixed points in the test particle picture has become a single, adiabatically evolving critical solution.

B. Equations of motion

In the extreme mass ratio limit, the larger object in the binary is approximated as a Schwarzschild black hole, and the lighter one as a particle moving in this background spacetime, with the equation of motion

$$u^b \nabla_b u^a = F^a, \quad (41)$$

where $u^b \nabla_b u^a = 0$ describes a geodesic on the background Schwarzschild spacetime, and F^a is the self-force per particle rest mass, which is proportional to the mass ratio η to leading order. (We use terminology customary in the self-force literature where it is really mE , mML and mF^a that have dimensions of energy, angular momentum and force.) ∇_a is the covariant derivative in the background spacetime, and indices are moved implicitly with the background metric.

As before, we define E and L by (10) and (11), and we impose the normalisation $u^a u_a = -1$ in the form (12). The time derivative of $u^a u_a = -1$ gives the usual constraint on any 4-force, namely

$$u_a F^a = 0. \quad (42)$$

From (41), we now have the 3-dimensional dynamical system

$$\ddot{r} = -\frac{1}{2} V_{,r}(L, r) + F^r, \quad (43)$$

$$\dot{L} = F_\varphi. \quad (44)$$

E can be read off as $E(r, \dot{r}, L)$ from (12), or can be evolved using the third component of (41), which can be written as

$$\dot{E} = -F_t. \quad (45)$$

These are compatible because of (42), which can be written as

$$\dot{r} F^r + E(F_t + \Omega F_\varphi) = 0, \quad (46)$$

where Ω is defined by (26). φ and t are evolved via (11) and (10).

C. Adiabatic expansion

By definition, the critical solution is the one that is balanced between plunging and running out to infinity. In the absence of radiation reaction, this clearly means it is a circular geodesic sitting on top of the potential. In the presence of radiation reaction, this definition becomes teleological: the critical solution hesitates as long as possible between plunging and running out to infinity. In practice we use adiabaticity to define the critical solution as being as circular or as stationary as possible: r should vary over a radiation reaction timescale, that is, \dot{r} should be proportional to the mass ratio η to leading order in the self-force expansion.

We formalize the adiabatic expansion through the series ansatz (slow-time expansion) [10]

$$F_*^a(\tau) = \sum_{k=1}^{\infty} \eta^k F_k^a(\hat{\tau}), \quad (47)$$

$$r_*(\tau) = \sum_{k=0}^{\infty} \eta^k r_k(\hat{\tau}), \quad (48)$$

$$L_*(\tau) = \sum_{k=0}^{\infty} \eta^k L_k(\hat{\tau}), \quad (49)$$

$$E_*(\tau) = \sum_{k=0}^{\infty} \eta^k E_k(\hat{\tau}), \quad (50)$$

where we have defined the slow time

$$\hat{\tau} := \eta\tau, \quad (51)$$

the suffix $*$ denotes the critical solution, and the normalisation condition (12) is obeyed order by order by virtue of (46). To leading order,

$$F_*^a = \eta F_1^a + O(\eta^2), \quad (52)$$

$$\ddot{r}_* = \eta^2 r_0'' + O(\eta^3), \quad (53)$$

$$\dot{L}_* = \eta L_0' + O(\eta^2), \quad (54)$$

$$\dot{E}_* = \eta E_0' + O(\eta^2). \quad (55)$$

where $\dot{f} := df/d\tau$ as before, and $f' := df/d\hat{\tau}$. Substituting this into (43,44), we obtain to leading order [$O(1)$ in (43), and $O(\eta)$ in (44)]

$$0 = V_{,r}(L_0, r_0) \quad \Rightarrow \quad r_0 = r_-(L_0), \quad (56)$$

$$L_0' = F_{\varphi 1}, \quad (57)$$

and this allows us to integrate r_0 and L_0 . Hence, $F_1^a(\hat{\tau}) = F_1^a(r_0(\hat{\tau}))$ is the first-order self-force on a circular geodesic orbit of radius r_0 , which is known [11]. To next order,

$$0 = -\frac{1}{2}[V_{,rr}(L_0, r_0)r_1 + V_{,rL}(L_0, r_0)L_1] + F_1^r, \quad (58)$$

$$L_1' = F_{\varphi 2} \quad (59)$$

formally give us r_1 and L_1 , but we cannot use this to calculate the critical solution beyond (r_0, L_0) . F_2^a is the second-order self-force. It comprises terms that are quadratic in metric perturbations and corrections due to the fact that the critical solution is not exactly geodesic. Both have not yet been calculated. Note, however, that (58) can be rewritten as

$$0 = -\frac{1}{2}V_{,r}(L_0 + \eta L_1, r_0 + \eta r_1) + \eta F_1^r + O(\eta^2), \quad (60)$$

and so its physical meaning is that the critical solution is slightly off the peak of the geodesic potential, held there (to this order) by the conservative part F_1^r of the self-force.

D. Self-force input

To leading order, our analysis requires knowledge of $\dot{L} = F_\varphi$ along circular orbits with $3 < r \leq 6$. In practice, we calculate $\dot{E} = -F_t$, which on circular orbits is related to \dot{L} by $\dot{L} = \dot{E}/\Omega$. To obtain \dot{E} we used the self-force code developed in Ref. [12], which is a frequency-domain variant of the original Barack-Sago code [11]. The code was originally developed to deal with stable orbits, but it can handle unstable (circular) orbits without any further development. The code takes as input the orbital radius r and returns the value of \dot{E} along that orbit. We have obtained accurate data for a dense sample of r values in the range $3 < r \leq 6$. The numerical data and details of their derivation are given in Appendix A.

Our numerical results can be approximated by the semi-heuristic fitting formula

$$\dot{E} \simeq -\eta r^{-5} z^{-\alpha} (a_0 + a_1 z + a_2 z^2 + a_3 z^3), \quad (61)$$

where $z := 1 - 3/r$ and the parameters

$$\begin{aligned} \alpha &\simeq 1.773163, & a_0 &\simeq 2.87683, & a_1 &\simeq -4.01414, \\ a_2 &\simeq 10.5371, & a_3 &\simeq -3.79087 \end{aligned} \quad (62)$$

have been determined by a least-squares fit of \dot{E} versus z . The r^{-5} decay at large r is well-known. We have modelled the blow-up of the self-force at the light ring by a single power $z^{-\alpha}$, although we have no rigorous theoretical argument for this. The numerical data we have fitted to are also not very close to the light ring, with the smallest value of r at 3.02, corresponding to $E \simeq 4.15$.

A tentative theoretical argument for determining α is that at sufficiently high energy the metric perturbation

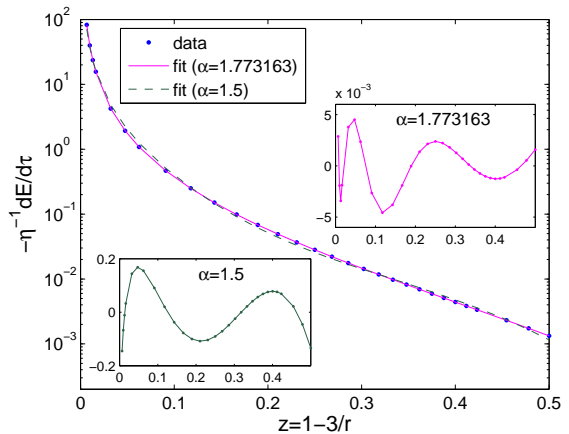


FIG. 3. Energy loss \dot{E}/η as a function of $z := 1 - 3/r$, for a circular geodesic orbit in the self-force approximation, and two closed-form fits. The fitting ansatz is given by Eq. (61) with α either fitted (solid line), or fixed at $\alpha = 3/2$ (dashed line). The self-force data (points) are given in Appendix A. The insets show the relative differences between the fit and the data for the two models (note the different vertical scales).

should be proportional to the total energy E of the particle and therefore the fluxes as seen by an observer at rest should be proportional to E^2 , so that

$$\dot{E} \sim \dot{t} E^2 \sim z^{-3/2}. \quad (63)$$

[Note that, from (10) and (27), $\dot{t} = z^{-1/2}$ on circular geodesics.] A least-squares fit to (61) where $\alpha = 1.5$ is held fixed results in a maximum fitting error of 17%. By comparison, the maximum fitting error with (62) is 0.5%, which is much smaller and comparable with the maximal estimated error of the self-force calculation (see Appendix A). The numerical self-force results and both fits are shown in Fig. 3. For our computations and plots in the remainder of the paper, we shall use the fit (61) with (62) for the range $r \geq 3.02$ for which we have self-force data, corresponding to $E \lesssim 4.15$.

Fig. 4 shows the energy absorbed by the large black hole as a fraction of the total energy loss (radiated to infinity plus absorbed by the large black hole). This figure is relevant for computing the total energy radiated to infinity, but not for our construction of the critical solution, where only the total energy loss matters.

E. Integration of the critical solution

In the presence of radiation reaction, for a given mass ratio η , there is a single critical solution where E , L , Ω , r , τ and φ are all monotonous functions of one another, with E and L decreasing from ∞ to finite values at plunge, r increasing from 3 to 6, and Ω decreasing from $3^{-3/2}$ to $6^{-3/2}$, all as τ and φ increase. In this paper we construct the critical solution only to leading order in η . Then E , L

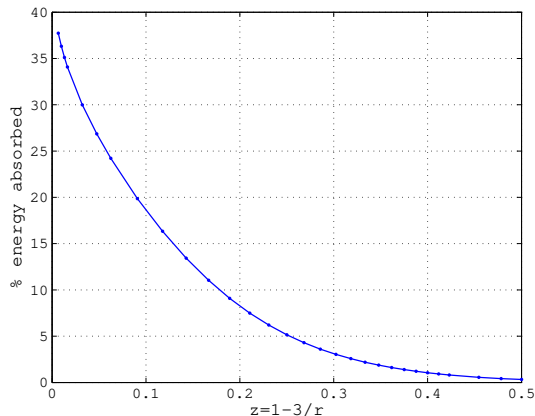


FIG. 4. The fraction of the total energy loss \dot{E}/η that is absorbed by the large black hole, as a function of $z := 1 - 3/r$. This is based on the data in Appendix A. Extrapolation gives a fraction of $\simeq 42\%$ at the light ring itself.

and Ω and r are known functions of one another, related by (27-29). Furthermore, the η -dependence of the critical solution is of the simple form $r = r(\hat{\tau}) = r(\hat{\varphi})$, where we define the “slow angle”

$$\hat{\varphi} := \eta\varphi \quad (64)$$

in analogy to the slow time $\hat{\tau}$. Finally, the ODEs obeyed by $\hat{\tau}(r)$ and $\hat{\varphi}(r)$ are separable, and can be solved by integration.

We obtain $\hat{\varphi}(r)$ by (numerical) integration of

$$\begin{aligned} \frac{d\hat{\varphi}}{dr} &= \eta \frac{d\varphi}{dt} \frac{dt}{d\tau} \frac{d\tau}{dE} \frac{dE}{dr} = \Omega \dot{t} \frac{dE}{dr} \frac{\eta}{\dot{E}} \\ &= \frac{1}{2} r^{-5/2} (r-3)^{-2} (r-6) \frac{\eta}{\dot{E}}, \end{aligned} \quad (65)$$

after substituting (61). A very good closed form approximation to this integral in terms of elementary functions can be obtained by approximating $(d\hat{\varphi}/dr)/(r-6)$ as a series in $(r-3)$ with three terms, multiplying back by $(r-6)$, and integrating this. The full result, the closed form approximation, and the ultrarelativistic approximation discussed below are shown in Fig. 5. For fixed η , this graph gives us the *shape* of the critical orbit.

We only have reliable self-force data for $r \geq 3.02$, corresponding to $E \lesssim 4.15$, but we are interested in the critical solution up to $E = \infty$. We have therefore extrapolated our fit (61) with (62) down to $r = 3$ in producing Fig. 5, and have used this extrapolation to set $\hat{\varphi}(3) = 0$ at $E = \infty$ as a matter of convention. Note, however, that almost the entire range of $\hat{\varphi}$ in this plot occurs for $r > 3.02$, where we do have reliable self-force data, with $\hat{\varphi}(3.02) \simeq 0.07$ compared to $\hat{\varphi}(6) \simeq 2.6$. This qualitative feature is robust, requiring only that \dot{E} diverges at the light ring faster than $(r-3)^{-1}$, that is $\alpha > 1$. Our self-force data for $r \leq 3.02$ support this qualitative feature robustly, with $\alpha \simeq 1.77$, while our crude theoretical model suggests $\alpha = 3/2$.

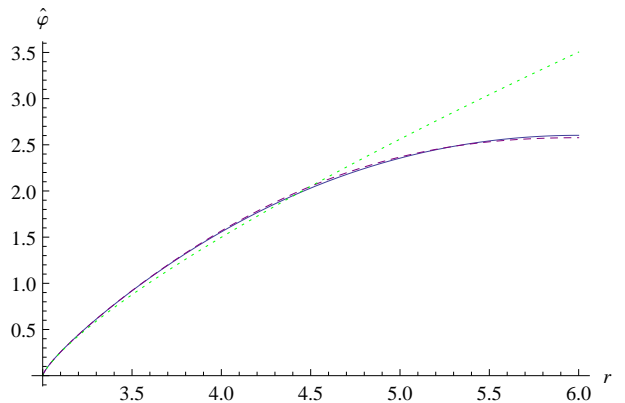


FIG. 5. Slow angle $\hat{\varphi}$ as a function of radius r in the critical solution. We have fixed $\hat{\varphi} = 0$ at $r = 3$. The full line represents a numerical integration of (65), with $\dot{E}(r)$ given by the fitting formula (61). The dashed line represents the closed form approximation discussed in the text below Eq. (65), and the dotted line the ultrarelativistic approximation (69). Note that here and in the following figure, the narrow section $r < 3 < 3.02$ of the domain is derived from an extrapolation of our self-force data.

Hence, the total number of orbits in the critical solution, from infinite energy down to plunge, is given by

$$n_{\text{tot}} = \frac{\hat{\varphi}(6)}{2\pi\eta} \simeq \frac{0.41}{\eta}, \quad (66)$$

and we expect the numerical prefactor to depend only weakly on our extrapolation of the self-force data.

We obtain $\hat{\tau}(r)$ by (numerical) integration of

$$\frac{d\hat{\tau}}{dr} = \frac{\eta}{\dot{E}} \frac{dE}{dr}. \quad (67)$$

A reasonably good closed form approximation for $\hat{\tau}(r)$ can be obtained by expanding $(d\hat{\tau}/dr)/(r-6)$ into a series in $(r-3)$ with four terms, multiplying back by $(r-6)$, and integrating. The full result and its approximations are shown in Fig. 6. Our self-force data suggest that $\hat{\tau}$, too, is finite at infinite energy, and we use the convention that $\hat{\tau} = 0$ at $E = \infty$. [From (67,30), the precise criterion is that $(r-3)^{-3/2}/\dot{E}$ is integrable.] Again, compare $\hat{\tau}(3.02) \simeq 0.02$ with $\hat{\tau}(6) \simeq 9.62$.

F. The ultrarelativistic approximation

In order to make quantitative statements about the critical solution beyond the energies covered by our self-force data, we shall assume that as $E \rightarrow \infty$, \dot{E} diverges like the leading order of (61), that is

$$\frac{\dot{E}}{\eta} \simeq -3^{\alpha-5} a_0 (r-3)^{-\alpha}. \quad (68)$$

(As discussed above, our qualitative conclusions that $\hat{\varphi}$ and $\hat{\tau}$ are finite at $E = \infty$ depend only on $(r-3)^{-2}/\dot{E}$ and

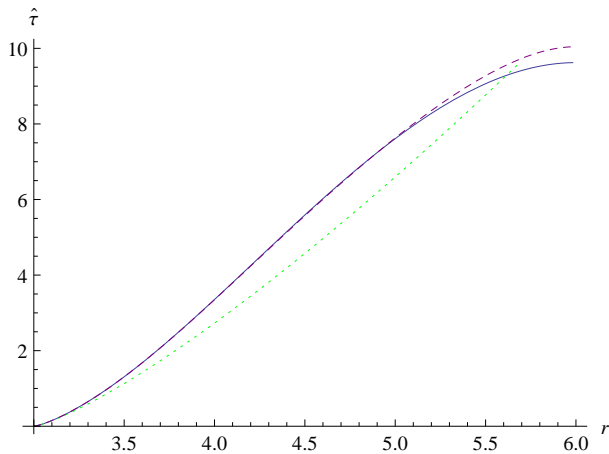


FIG. 6. Slow time $\hat{\tau}$ as a function of radius r in the critical solution. We have fixed $\hat{\tau} = 0$ at $r = 3$. The full line represents a numerical integration of (67). The dashed line represents the closed form approximation for $\hat{\tau}(r)$ discussed in the text below Eq. (67) and the dotted line the ultrarelativistic approximation (70).

($r - 3$) $^{-3/2}/\dot{E}$ being integrable as $r \rightarrow 3$.) We shall refer to calculations where we only use the leading power of $(r - 3)$ throughout as the ultrarelativistic approximation, and in this context we shall treat $a_0 > 0$ and $\alpha > 1$ as undetermined.

Combining the leading order of (65) with (68) and integrating, we obtain

$$\hat{\varphi}(r) \simeq \frac{3^{7/2-\alpha}}{2a_0(\alpha-1)}(r-3)^{\alpha-1}, \quad (69)$$

Similarly, taking the leading power of $(r - 3)$ in (67), we obtain

$$\hat{\tau}(r) = \frac{3^{9/2-\alpha}}{a_0(2\alpha-1)}(r-3)^{\frac{2\alpha-1}{2}}. \quad (70)$$

In the ultrarelativistic approximation we can combine (30) with (69) and (70) to express $r - 3$, $\hat{\tau}$, $\hat{\varphi}$ and E all as powers of each other. In particular

$$E(\hat{\tau}) \simeq C_E \hat{\tau}^{-\beta}, \quad (71)$$

where

$$C_E := [3^{2\alpha-5} a_0 (2\alpha - 1)]^{-\beta}, \quad \beta := \frac{1}{2\alpha - 1} \quad (72)$$

which will be used later. With

$$\dot{\varphi} \simeq \frac{E}{\sqrt{3}} \quad (73)$$

in the ultrarelativistic approximation, we also have

$$\hat{\varphi} \simeq \frac{C_E}{\sqrt{3}(1-\beta)} \hat{\tau}^{1-\beta} \simeq \frac{C_E^{1/\beta}}{\sqrt{3}(1-\beta)} E^{1-1/\beta}. \quad (74)$$

In the ultrarelativistic limit (40) becomes

$$\Gamma \simeq \frac{9}{L} \simeq \frac{\sqrt{3}}{E} \simeq \frac{\sqrt{3}}{C_E} \hat{\tau}^\beta, \quad (75)$$

where we have used (71) in the last equality.

G. Validity of the self-force and adiabatic approximations

The self-force approximation to the equations of motion is valid when the total energy mE of the small object is much smaller than the total energy M of the large black hole, that is, for

$$E \ll \eta^{-1}. \quad (76)$$

Because the self-force diverges as $E \rightarrow \infty$ at fixed η , we must also estimate where the adiabatic approximation breaks down at high energy. Heuristically, we assume that the adiabatic approximation is valid if E changes at most by some small fraction $\delta \ll 1$ per orbit, or

$$-\frac{d \ln E}{d \hat{\varphi}} \ll \frac{\delta}{2\pi\eta}. \quad (77)$$

(The explicit η on the right comes from the hat on the left.) From (74), we find that in the ultrarelativistic regime this is equivalent to

$$E \ll \left(\frac{\eta}{\delta}\right)^{-\frac{1}{2\alpha-2}}. \quad (78)$$

We see that the adiabaticity condition (78) always implies the condition (76) for the self-force approximation itself to be valid if $\alpha \geq 3/2$. (Recall our theoretically motivated value of α is $3/2$, and our fitted value is 1.77 .)

Note that the adiabatic approximation breaks down also as the plunge is approached, because the effective potential becomes shallower, leading to a rapid increase in r_1 at finite F^r in (58) [13].

V. CRITICAL SCALING IN THE SELF-FORCE APPROXIMATION

A. Perturbations of the critical solution

We now consider a small perturbation of the critical solution that results from imperfect fine-tuning of the initial data, as discussed above in Sec. II, namely

$$r = r_*(\hat{\tau}) + \delta r(\tau), \quad L = L_*(\hat{\tau}) + \delta L(\tau), \quad (79)$$

where r_* and L_* are given by the adiabatic ansatz (48,49) above, while δr and δL are just functions of τ , that is, they are assumed to remain “fast” even in the limit of weak radiation reaction. The self-acceleration is perturbed as

$$F^a = F_*^a + O(\eta)O(\delta r, \delta L), \quad (80)$$

where the factor η arises simply because any self-acceleration scales as $O(\eta)$. Substituting this into the equations of motion and subtracting the critical solution, we formally obtain

$$\delta\ddot{r} = -\frac{1}{2}[V_{,rr-}(L_0, r_0)\delta r + V_{,rL}(L_0, r_0)\delta L] + O(\delta r^2, \delta L^2, \delta r\delta L) + O(\eta)O(\delta r, \delta L), \quad (81)$$

$$\delta\dot{L} = O(\eta)O(\delta r, \delta L). \quad (82)$$

We now neglect the error terms above, the first set as they are nonlinear in $(\delta r, \delta L)$, the second set as they are small corrections to the *coefficients* of a linear differential equation for $(\delta r, \delta L)$.

In identifying the perturbed solution with the background critical solution, we can adjust the origin of τ in the perturbed solution. (This is a remnant of the usual gauge-dependence of spacetime perturbations.) As $L_*(\hat{\tau})$ is not constant, we can use this to set $\delta L = 0$ at any one time, and hence, by $\delta\dot{L} \simeq 0$, at all times. Note that the neutral mode $\delta L = \text{constant}$ present in the geodesic approximation, which linked neighbouring critical solutions, has become a gauge mode in the presence of radiation reaction, where there is a single critical solution, and that we have used a simple form of gauge fixing to eliminate this mode. From now on we denote δr in this gauge by x . We are left with the single equation of motion

$$\ddot{x} \simeq \Gamma(\hat{\tau})^{-2}x, \quad (83)$$

which is equivalent to (37) for the geodesic case, but where now

$$\Gamma(\hat{\tau}) := \Gamma[L_0(\hat{\tau})] \quad (84)$$

is time-dependent.

Rewriting the equation entirely in terms of $\hat{\tau}$, we have

$$x'' \simeq \eta^{-2}\Gamma(\hat{\tau})^{-2}x, \quad (85)$$

where as before a prime denotes $d/d\hat{\tau}$. As η is small, we can use a WKB approximation. In terms of the ‘‘WKB time’’

$$T(\hat{\tau}) := \int \frac{d\hat{\tau}}{\Gamma(\hat{\tau})}, \quad (86)$$

where for definiteness we let $T(0) = 0$, the first-order WKB approximation to the growing and decaying solutions is

$$x_{\pm}(\hat{\tau}) \simeq \sqrt{\Gamma(\hat{\tau})}e^{\pm\eta^{-1}T(\hat{\tau})}. \quad (87)$$

This is a good approximation for $|\dot{\Gamma}| \ll 1$, when the prefactor varies much more slowly than the exponential. The functions $\Gamma(\hat{\tau})$ and $T(\hat{\tau})$ are shown in Figs. 7 and 8.

In the ultrarelativistic approximation, from (75), we have

$$T \simeq \frac{C_E}{\sqrt{3}(1-\beta)}\hat{\tau}^{1-\beta} \simeq \frac{C_E^{1/\beta}}{\sqrt{3}(1-\beta)}E^{1-1/\beta} \simeq \hat{\varphi}, \quad (88)$$

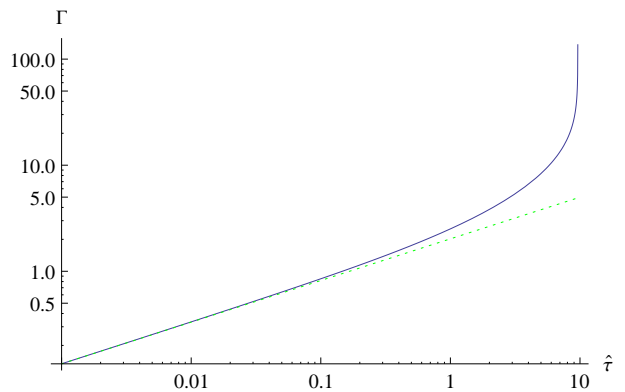


FIG. 7. Log-log plot of $\Gamma(\hat{\tau})$ [defined in (40), based on (61,62) (solid line), and the ultrarelativistic approximation (75) (dotted line). (The divergence of Γ comes from the shallowness of the potential at $r = 6$.)

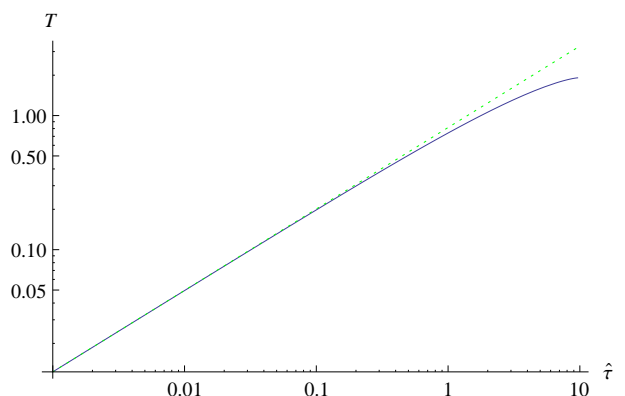


FIG. 8. Log-log plot of $T(\hat{\tau})$ [defined in (86), based on (61,62) (solid line), and the ultrarelativistic approximation (88) (dotted line).

where we have used (74) in the last two equalities. In the same approximation,

$$\dot{\Gamma} \simeq \sqrt{3}\beta C_E^{1-2\alpha}\eta E^{2\alpha-2}. \quad (89)$$

Hence $|\dot{\Gamma}| \ll 1$ for

$$E \ll \eta^{-\frac{1}{2\alpha-2}}, \quad (90)$$

which has the same power of η as the criterion (78) for the critical solution to evolve adiabatically. Clearly, with $\delta < 1$, (78) implies (90) and hence, for $\alpha \geq 3/2$, also (76). Hence the only criterion we need to impose is (78) (the critical solution evolves adiabatically), and we can then always use the WKB approximation to the critical solution.

For τ small enough (E large enough) that $|\dot{\Gamma}| \gg 1$, the WKB approximation does not hold. However, we are then necessarily in the ultrarelativistic limit such that the approximation (75) for $\Gamma(\hat{\tau})$ holds, and with this, (83) can be solved in closed form in terms of Bessel functions. As this result is not directly relevant for our main result, we give it in Appendix B.

B. Dependence on the initial data

For definiteness, we parameterise the space of initial data (modulo a shift in time) by the initial energy at infinity E_i and the impact parameter b . We consider a generic near-critical solution in the whirl phase $\tau_i < \tau < \tau_f$ where it is close to the critical solution, so that

$$x(\tau) \simeq A(E_i, b) \frac{x_-(\tau)}{x_-(\tau_i)} + B(E_i, b) \frac{x_+(\tau)}{x_+(\tau_i)}. \quad (91)$$

The factors $x_{\pm}(\tau_i)$ have been introduced for later convenience.

A and B are smooth functions of E_i and b , and by definition B vanishes for critical initial data. Therefore,

$$A = A_0(E_i) + O(\delta b), \quad B = B_1(E_i)\delta b + O(\delta b)^2, \quad (92)$$

where

$$\delta b := b - b_*(E_i, \eta). \quad (93)$$

[The critical value $b_*(E_i, \eta)$ of the impact parameter is known in closed form only for $\eta = 0$, when it is given by (33), but its value does not matter in the following.] We must have $A > 0$ and $B_1 > 0$ because x is positive and decreasing during the approach to the critical solution, and then becomes negative in the capture case $b < b_*$, or returns to large positive values in the scattering case $b > b_*$.

Let the beginning and end of the whirl phase be defined by $x(\tau_i) = X_i$ and $x(\tau_f) = X_f$, where X_i and X_f will be characterised later. If the whirl phase is sufficiently long, we can neglect the growing mode at τ_i and the decaying mode at τ_f , so that

$$A_0 \simeq X_i, \quad (94)$$

$$B_1 \delta b \simeq X_f \frac{x_+(\tau_i)}{x_+(\tau_f)}. \quad (95)$$

Note that X_i is always positive, while X_f is positive for initial data that scatter and negative for initial data that plunge.

In the general discussion of critical scaling in Sec. II, we introduced two constants C_1 and C_2 that were treated as unknown, and combined into a constant C_3 in the final result (4). The equivalents of C_1 and C_2 in the current specific problem are B_1 and X_f , respectively, and we shall now see that under certain conditions we can determine both, so that there is no undetermined constant left in our final results.

In order to determine B_1 we can use an energy argument if we approximate E as constant during the approach phase. This is justified when the energy loss during the approach phase is small compared to the energy loss during an extended whirl phase. We approximate (87) over a short time interval (covering the transition from approach to whirl) as

$$x_{\pm}(\tau) \simeq e^{\pm(\tau-\tau_i)/\Gamma(\tau_i)} x_{\pm}(\tau_i). \quad (96)$$

Perturbing (12), which holds for geodesics, with respect to b , we obtain

$$E^2(L, b) - E_*^2(L) \simeq \dot{x}^2 - \Gamma^{-2}x^2 \simeq -4\Gamma^{-2}AB, \quad (97)$$

where the last equality follows from (96). This equation becomes exact in the geodesic limit, where E is conserved and (96) is exact. On the other hand, when E is conserved, from (25) we also have

$$E^2(L, b) - E_*^2(L) \simeq -\frac{2L^2}{b_*^3} \delta b \simeq -2[E_*^2(L) - 1] \frac{\delta b}{b_*}. \quad (98)$$

Note the factor $E^2 - 1$ in dE/db . It comes about because geodesic orbits with $E = 1$ are at rest at infinity, and so the impact parameter is not defined. More concretely, displacing a particle at rest at infinity in a direction orthogonally to the line of sight to the large black hole before dropping it corresponds to a rotation of the binary system and makes no difference to the infall. Because of this factor, some of our following results will be formally singular at $E = 1$. This is only because b becomes a bad parameter of the initial data. In practice, we are interested in initial data with $E > 1$ (and in particular $E \gg 1$), when this is not a problem.

We now approximate $E_*(L) = E_i$ in (98) and $\Gamma \simeq \Gamma[L_*(E_i)] =: \Gamma_i$ in (97) because we approximate E and L as constant for $\tau < \tau_i$ and because $L_i \simeq L_*(E_i)$ by fine-tuning. Hence we find

$$A_0 B_1 \simeq \frac{\Gamma_i^2 (E_i^2 - 1)}{2b_*}. \quad (99)$$

From (94), (95) and (99), and taking the logarithm for later convenience, we now obtain

$$-\ln \frac{|\delta b|}{b_*} - \ln \left| \frac{\Gamma_i^2 (E_i^2 - 1)}{2X_i X_f} \right| \simeq \ln \frac{x_+(\tau_f)}{x_+(\tau_i)}. \quad (100)$$

This is our master equation for critical scaling: in principle, it determines E_f in terms of the mass ratio η and the initial data (E_i, b) . In order to obtain a definite result, however, we still need to fix X_i and X_f . As we discuss below, there is a natural criterion for fixing them in the radiation reaction, but only a more arbitrary one in the geodesic limit. Moreover, the criterion we choose in the radiation reaction case has a singular limit as $\eta \rightarrow 0$ in the geodesic limit. We therefore discuss both cases separately, starting with the geodesic case.

C. Critical exponents in the geodesic case

The critical solution is by definition as circular as possible in the presence of radiation reaction, sitting approximately at the top of the potential. Hence one possible criterion for X_i and X_f is that the radial velocity be a given small fraction C_e (for ‘‘eccentricity’’) of the tangential velocity, or

$$\left(\frac{|\dot{x}|}{r\dot{\varphi}} \right)_{i,f} = C_e. \quad (101)$$

Note that C_e plays the role of C_2 in our general discussion in Sec. II, and while it must be small, its choice is arbitrary – we have introduced it here because it is more intuitive than $X_{i,f}$. We have

$$\left(\frac{|\dot{x}|}{r\dot{\phi}}\right)_{i,f} \simeq \frac{\sqrt{E^2 - V}}{r^{-1}L} \simeq \frac{|X_{i,f}|}{\Gamma r^{-1}L} \simeq \frac{|X_{i,f}|}{\sqrt{3}\Gamma E}, \quad (102)$$

where we have used (11) and (12) in the first step, (40) in the second step, and the third approximation holds only in the ultrarelativistic limit.

In the geodesic case, where the background solution is time independent,

$$x_{\pm} = e^{\pm\tau/\Gamma} \quad (103)$$

holds exactly. Using this and (100-102), we obtain

$$\tau_f - \tau_i \simeq -\Gamma \ln \frac{|\delta b|}{b_*} - \Gamma \ln \tilde{C}_e. \quad (104)$$

where Γ is given by (40). Here

$$\tilde{C}_e := \frac{E^2 - 1}{2C_e^2 r^{-2} L^2} = \frac{4 - r}{2C_e^2 r} \simeq \frac{1}{6C_e^2}, \quad (105)$$

where the last approximate equality holds only in the ultrarelativistic limit $r \simeq 3$. Clearly, \tilde{C}_e inherits the arbitrariness of C_e . The result (104) can be expressed in terms of orbits as

$$n \simeq -\gamma \ln \frac{|\delta b|}{b_*} - \gamma \ln \tilde{C}_e, \quad (106)$$

where

$$\gamma := \frac{\dot{\phi}}{2\pi} \Gamma = \frac{L^{1/2}}{2\pi L_{12}^{1/2}} \quad (107)$$

In the ultrarelativistic limit, we have

$$\Gamma \simeq \frac{\sqrt{3}}{E}, \quad (108)$$

$$\gamma \simeq \frac{1}{2\pi}. \quad (109)$$

The critical exponents Γ and γ for the geodesic limit were previously obtained by Pretorius and Khurana [2] for equatorial geodesics of Kerr, and had previously been given, in different notation, in Eq. (2.25) of [8]. The additive constant parameterised by C_e could only be determined more exactly by a full modelling of the perturbed orbit to replace the artificial split into a zoom-in, whirl and zoom-out or plunge phase.

As an extension of the result for the time spent whirling, we can – trivially – estimate the energy loss during the whirl phase as

$$\Delta E \simeq (\tau_f - \tau_i) \dot{E}(E_i), \quad (110)$$

where $(\tau_f - \tau_i)$ is given in terms of the initial data by (104) and the constant $\dot{E}(E_i)$ is given implicitly by relating E_i to r using the exact formula (27) for the energy

on a circular orbit and \dot{E} to r using our numerical result (77) for the energy loss on circular geodesics. This approximation, where we neglect the radiation reaction on the orbit itself, is therefore consistent only for $\Delta E \ll E_i$. (110) complements the results given in [4] for the energy radiated in the geodesic approximation scattering orbits not close to the threshold of immediate merger.

D. Generalised critical scaling in the radiation reaction case

With radiation reaction, a less arbitrary definition of X_i and X_f is given by equating the rate of change of the perturbation x with that of the background solution, that is

$$|\dot{x}| \simeq |\Gamma_{i,f} X_{i,f}| \simeq \dot{r}_*. \quad (111)$$

Furthermore, we have seen above that we can always use the WKB approximation (87) to the perturbation modes when the adiabatic self-force approximation to the background critical solution is valid. Substituting our new definition (111) of $X_{i,f}$ into the left-hand side of the scaling master equation (100), and the WKB approximation (87) into its right-hand side, (100) becomes

$$-\ln \frac{|\delta b|}{b_*} - \ln \frac{\Gamma_i^3 \Gamma_f (E_i^2 - 1)}{2\eta^{-2} r'_{0i} r'_{0f}} \simeq \frac{T_f - T_i}{\eta} + \frac{1}{2} \ln \frac{\Gamma_f}{\Gamma_i}. \quad (112)$$

We can re-order this as

$$-\ln \frac{|\delta b|}{b_*} \simeq \frac{T_f - T_i}{\eta} + 2 \ln \eta + K_i + K_f, \quad (113)$$

where we have defined the shorthands

$$K_i := \ln \frac{\Gamma_i^{5/2} (E_i^2 - 1)}{2r'_{0i}}, \quad (114)$$

$$K_f := \ln \frac{\Gamma_f^{3/2}}{r'_{0f}}. \quad (115)$$

Here we consider T , K_i and K_f as functions of $\hat{\tau}$ (or any of the other slow variables E , r , $\hat{\phi}$). The only η -dependence is then the one explicitly shown in (113).

Alternatively, we can re-order (113) as

$$\frac{T_f}{\eta} + K_f \simeq -\ln \frac{|\delta b|}{b_*} + \frac{\hat{T}_i}{\eta} - K_i - 2 \ln \eta. \quad (116)$$

This gives a known function of $\hat{\tau}_f$ (or E_f), on the left-hand side, as a known function of the mass ratio η and the initial data (E_i, b_i) , on the right-hand side. To fully expand this in terms of E_f and E_i , we first note that (27) gives an expression for $E(r)$ that can be inverted to obtain $r(E)$. (40) gives $\Gamma(L)$ and (28) gives $L(r)$, so that we can explicitly obtain $\Gamma(E)$. (We do not give the

expression here, as it is unwieldy.) Next we note that (67) can be rewritten as

$$r'_0(r) = [\eta^{-1} \dot{E}](r) \left(\frac{dE}{dr} \right)^{-1}, \quad (117)$$

where $r'_0 := dr_0/d\hat{\tau}$ as before. Finally we note that the definition (86) of $T(\hat{\tau})$ can be rewritten as

$$T(r) = \int \frac{dr}{r'_0(r)\Gamma(r)}, \quad (118)$$

which can then be written as $T(r(E))$, or directly as

$$T(E) = \int \frac{dE}{r'_0(r(E))\Gamma(r(E))\frac{dE}{dr}(r(E))}. \quad (119)$$

With the definitions (114,115) of K_i and K_e in terms of Γ , E and r'_0 , we can now write our master equation (116) in terms of the mass ratio η , the initial data (E_i, b) , and the final energy E_f , subject to evaluating the integral in either (118) or (119). However, this equation cannot be solved for $E_f = E_f(\eta, E_i, b)$ in closed form.

We can make (116) more explicit, in terms of only powers and logarithms, when the entire whirl phase is ultrarelativistic, that is $E_f \gg 1$. We have already given the ultrarelativistic approximations for $T(\hat{\tau})$, $\hat{T}(E)$ and $T(\hat{\varphi})$ in (88), and we similarly find that that in the ultrarelativistic limit

$$K_i \simeq -2 \ln 2 + \left(\frac{3}{4} + 6\beta \right) \ln 3 - \frac{3\beta}{2} \ln a_0 + \left(1 - \frac{3\beta}{2} \right) \ln \frac{\hat{\tau}}{\beta}, \quad (120)$$

$$K_f \simeq -\ln 2 + \left(\frac{5}{4} + 2\beta \right) \ln 3 - \frac{\beta}{2} \ln a_0 + \left(1 - \frac{\beta}{2} \right) \ln \frac{\hat{\tau}}{\beta}. \quad (121)$$

[These can be readily re-expressed in terms of $\hat{\varphi}$, E , or $(r-3)$ using (69-71).] We have plotted $T(\hat{\tau})$ above in Fig. 8, and we plot $K_i(\hat{\tau})$ and $K_f(\hat{\tau})$ in Figs. 9 and 10, all based on (61,62) and each compared against its ultrarelativistic approximation. Fig. 11 plots all three against E instead of $\hat{\tau}$.

Note from Fig. 11 that $\ln T$, K_i and K_f vary comparably rapidly along the critical solution, but it is T/η (without the logarithm), K_i and K_f that appear in our scaling result (113). Hence one can suppress K_i and K_f in (113) as logarithmic corrections relative to the T terms. Doing this, suppressing also the constant term $2 \ln \eta$, and taking the ultrarelativistic limit for clarity reduces (113) to

$$-\ln \frac{|\delta b|}{b_*} \simeq \frac{T_f - T_i}{\eta} \quad (122)$$

$$\simeq \eta^{-\beta} \frac{C_E}{\sqrt{3}(1-\beta)} \left(\tau_f^{1-\beta} - \tau_i^{1-\beta} \right) \quad (123)$$

$$\simeq \eta^{-1} \frac{C_E^{1/\beta}}{\sqrt{3}(1-\beta)} \left(E_f^{1-1/\beta} - E_i^{1-1/\beta} \right) \quad (124)$$

$$\simeq \varphi_f - \varphi_i. \quad (125)$$

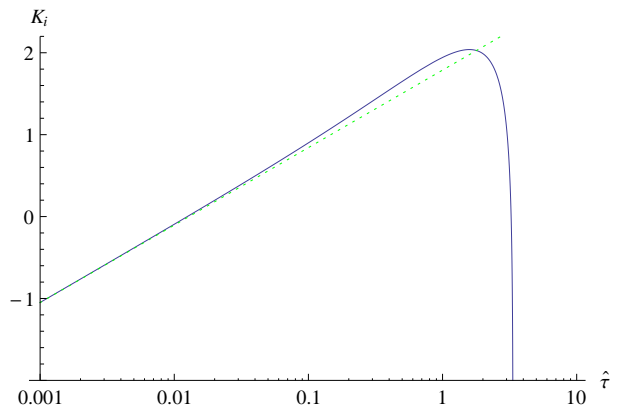


FIG. 9. Log-linear plot of $K_i(\hat{\tau})$ [defined in (114), based on (61,62) (solid line), and the ultrarelativistic approximation (120) (dotted line). The full curve ends because of the factor $E^2 - 1$ in the exact expression, which is approximated as E^2 in the ultrarelativistic expression

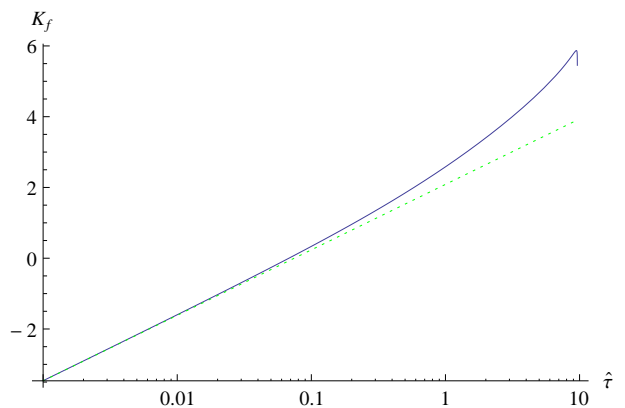


FIG. 10. Log-linear plot of $K_f(\hat{\tau})$ [defined in (115), based on (61,62) (solid line), and the ultrarelativistic approximation (121) (dotted line).

It is interesting to note that the amount of fine-tuning of the initial data (measured by $\ln |\delta b|$) required to achieve a given number of orbits on the critical solution is independent (within the self-force approximation) of the mass-ratio η . [In particular, the limit $\eta \rightarrow 0$ of (125) is trivial and gives (106) with (109).] By comparison, better fine-tuning (smaller $|\delta b|$) is required to achieve a given time on the critical solution, or a given amount of energy radiated, as η becomes smaller. These scalings with η are not immediately intuitive.

Finally, to see how the self-force result is related to the geodesic limit, we go back to (112). The second term on the left-hand side comes from the criterion (111) for determining X_i and X_f , and is simply not defined when the self-force is neglected. (Formally, it diverges as $\eta \rightarrow 0$.) In the geodesic case we therefore adopted the more ad-hoc definition (101) of X_i and X_f . Hence, in the geodesic limit the left-hand side of (112) becomes $-\ln(|\delta b|/b_*)$ plus some constant related to X_i and X_f

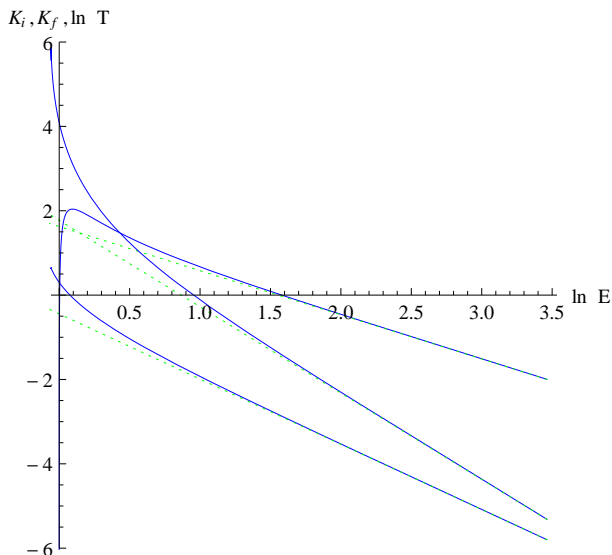


FIG. 11. Plot of (from top to bottom at large E) K_i , K_f and $\ln T$ (note the logarithm), all versus $\ln E$, based on (61,62) (solid lines), and the corresponding ultrarelativistic approximations (dotted lines).

but independent of δb . On the right-hand side of (112), we note $\Gamma_i = \Gamma_f =: \Gamma$, so the second term vanishes, and from (86) we have

$$\lim_{\eta \rightarrow 0} \frac{T_f - T_i}{\eta} = \frac{\tau_f - \tau_i}{\Gamma}. \quad (126)$$

Hence we recover (104) as the $\eta \rightarrow 0$ limit of (112), but with the constant \tilde{C}_e undetermined by (112).

VI. CONCLUSIONS

Pretorius and Khurana [2] suggested equatorial zoom-whirl orbits in Kerr as a toy model for the critical phenomena at the threshold of immediate merger in equal mass black hole binaries that they had observed in numerical relativity simulations. Here, we have adapted this toy model to make *quantitative* predictions in the limit where one of the two black holes is much larger than the other. We can then model the smaller black hole as a point particle of mass m in a background spacetime given by the larger one (assumed to be Schwarzschild with mass $M = 1$), and moving on an orbit determined by a gravitational self-force proportional, to leading order, to the mass ratio $\eta := m/M \ll 1$.

In our model there is a single critical solution that evolves adiabatically along the sequence of unstable circular geodesics, beginning with infinite energy and ending with a plunge when almost all the energy has been dissipated in gravitational waves. In this process, the critical orbit evolves from $r = 3$ and $E = \infty$ (the light ring) to $r = 6$ and $E = \sqrt{8/9}$ (the last stable circular or-

bit), making only a finite number (approximately $0.41/\eta$) of orbits.

Any initial data fine-tuned to the critical impact parameter are attracted to the critical solution, joining it at the appropriate energy. They leave it after a number of orbits determined by the degree of fine-tuning, to either plunge or scatter. Beyond a certain degree of fine-tuning, they stay on the critical solution until it plunges.

The type of critical solution we have described here is unfamiliar in general relativity, being neither self-similar (type II) nor stationary (type I). Rather, it avoids immediate plunge or scatter by remaining as circular as is compatible with radiation reaction. The appropriate symmetry ansatz is therefore a formal slow time expansion, in which the orbit evolves adiabatically from one circular geodesic orbit to an adjacent one under the effect of energy and angular momentum loss. We might call this type Ia, for “adiabatic”.

The fact that a type Ia critical solution evolves because of dissipation makes no essential difference to the dynamical systems picture, where the critical solution is defined as balanced between two basins of attraction. The conjecture in [16] that “zoom-whirl behaviour has better odds at surviving dissipation [for smaller η] because of the slower dissipation time” is not supported by this picture, and in fact Eq. (125) shows that the dependence of the whirl angle on the fine-tuning of the initial data is independent of η in the ultrarelativistic limit.

Our main result links the final energy (per rest mass) E_f of the small object to its initial energy E_i , the impact parameter b and the mass ratio η . This is given in implicit form in our master equation (116) – see also the discussion in the paragraph following this equation. We have also given more explicit approximate expressions (neglecting subleading terms, and assuming for clarity that $E_f \gg 1$) in Eqs. (123-125).

For the purpose of our calculation, there are four different regimes for the initial energy:

1) For $\sqrt{8/9} < E_i \lesssim 4$ we have accurate self-force data and so our results are reliable, but cannot be expressed in closed form. (We plot them, and the interested reader could reconstruct all our plots from the data and formulas given in this paper.) Even in this regime, we had to extend previous self-force calculations much closer to the light ring at $r = 3M$, and it is clear that the self-force diverges there. It would be highly interesting in its own right to understand the origin of this divergence rigorously.

2) For $4 \lesssim E_i \lesssim \eta^{-1/(2\alpha-2)}$, we are extrapolating our numerical self-force data for \dot{E} as $(r-3)^{-\alpha}$, see Eq. (68). (A best fit to our numerical data gives $\alpha \simeq 1.77$, but we also have a heuristic theoretical argument for $\alpha = 3/2$, which is a less good fit but not obviously wrong, see Fig. 3.) In this regime the motion is ultrarelativistic, which allows us to give explicit expressions. As η can be arbitrarily small, we give our (extrapolated) results up to $E_i = \infty$.

3) If $\alpha < 3/2$, there is an even higher energy regime

$\eta^{-1/(2\alpha-2)} \lesssim E_i \lesssim \eta^{-1}$ when the self-force approximation is still valid, but the adiabatic approximation is not. (This regime is empty for $\alpha \geq 3/2$.) It should be possible to calculate in this regime in the foreseeable future, but at the moment of writing this, the gravitational self-force on non-geodesic orbits in the Schwarzschild spacetime has not yet been calculated. (Similarly, it should become possible in the foreseeable future to extend our self-force results to the case where the large black hole is Kerr.)

4) Finally, for $E_i \gtrsim \eta^{-1}$, the (total, mostly kinetic) energy of the small particle becomes comparable to that of the large black hole, and the self-force approximation itself breaks down. (We come back to this regime just below.)

Two surprising features of the critical solution at the threshold of immediate merger, at least in the extreme-mass ratio approximation, are its unfamiliar (approximate) symmetry, and the fact that the *fraction* of E radiated per orbit increases with E fast enough that the critical solution evolves from $E = \infty$ (or at least from $E \sim \eta^{-1} \gg 1$, for any fixed finite mass ratio η) to plunge at $E \simeq \sqrt{8/9}$ in a finite number of orbits.

We conjecture that both these qualitative features hold also in the comparable to equal mass ratio case. Evidence that the fraction of energy radiated per orbit increases with energy is given by comparing the numerical relativity results of [2] (1.0 – 1.5% at a boost of $k \simeq 0.22$) and [7] ($\sim 13\%$ at a boost of $k \simeq 1.5$ [14]). We should stress again that for any given mass ratio η (and spins) there is only one critical solution, which begins with infinite energy. We also conjecture that this solution radiates an infinite amount of energy over a finite, probably quite small, number of orbits. At low energies, an adiabatic approximation should be possible, where the critical solution evolves along a sequence of stationary solutions with a helical Killing vector under the influence of radiation reaction, but if our conjecture is correct this breaks down at sufficiently large energy.

In the comparable mass case, the dependence of the orbital radius of the critical solution on the energy will be very different from that in the extreme mass ratio case. For two point masses $M_1 := M$ and $M_2 := \eta M$ in special relativity, where we set $\eta \leq 1$ by definition, with a relative boost $k := -u_1^a u_{2a} \geq 1$ towards each other, the total energy in their common centre of mass frame is given by

$$E_{\text{CM}} = M \sqrt{1 + 2\eta k + \eta^2}. \quad (127)$$

Furthermore, the hoop conjecture suggests that the critical impact parameter for immediate merger is

$$b_* \sim E_{\text{CM},i}, \quad (128)$$

and this is borne out by numerical relativity simulations for comparable masses and large k [15]. Finally, as the critical solution is by definition always between scattering and merger, we also expect

$$r_*(t) \sim E_{\text{CM}}(t) \quad (129)$$

along the critical solution. In the limit $k\eta \gg 1$, (128) gives us $b_* \sim M\sqrt{2\eta k}$ and from (129) the critical solution *spirals in* from infinite orbital radius to the innermost stable circular orbit (ISCO). In the opposite limit $k\eta \ll 1$, (128) gives us $b_* \sim M$ (a more precise result is of course $b_* \simeq 3\sqrt{3}M$), the self-force approximation we have given here becomes valid, and the critical solution *spirals out* from the light ring to the ISCO.

Constructing the critical solution presents a challenge at any mass-ratio: for self-force methods in the extreme mass-ratio case to reach higher energies and to go beyond the adiabatic approximation to the orbit, and for effective one-body and numerical relativity methods in the comparable mass ratio case to construct the critical solution even at low energies.

ACKNOWLEDGMENTS

We thank Nori Sago for using his code to test some of our self-force data. CG, SA and LB acknowledge support from STFC through grant numbers PP/E001025/1 and ST/J00135X/1.

Appendix A: Numerical data

We present here the numerical data used to inform our “empirical” formula (61) for $\dot{E}(r)$. The data were generated using the self-force code developed by Akcay in Ref. [12]. The code computes \dot{E} in two different ways: (i) Directly, by calculating the component F_t of the local gravitational self-force (per unit particle mass m) and using $\dot{E} = -F_t$; and indirectly, by numerically evaluating the flux of energy in gravitational waves radiated to infinity and down the event horizon, and using the energy balance relation $-\dot{E} = (dE_{\text{GW}}/dt)(dt/d\tau)$. Here dE_{GW}/dt is the total flux of energy (per m) carried by the gravitational waves, and $dt/d\tau = (1 - 3/r)^{-1/2}$. dE_{GW}/dt is made up of two pieces, dE_{GW}^+/dt and dE_{GW}^-/dt , respectively associated with radiation going out to infinity and absorbed by the black hole. The numerical evaluation of both F_t and dE_{GW}^\pm/dt are detailed in Ref. [12]. We find that the two computations agree extremely well, differing by no more than one part in $\sim 10^{10}$ for $r \geq 3.2$. At smaller radii the agreement is less good, but for none of the radii we considered (down to $r = 3.02$) is the disagreement greater than 1%.

There is a practical limit on how close to $r = 3$ our numerical method can reach. Both above computations (of the local self-force and of the asymptotic fluxes) rely on a summation over multipole-mode contributions, with a practical cut-off at some $l = l_{\text{max}}$. Our calculations typically use $l_{\text{max}} \simeq 80$ for the self-force and $l_{\text{max}} \simeq 140$ for the fluxes. As the (ultra-relativistic) limit $r \rightarrow 3$ is approached, a beaming-like effect broadens the l -mode power distribution and shifts it toward large l . For $r - 3$ small enough it becomes computationally prohibitive to

obtain a sufficient number of modes. In practice, we have not attempted to obtain accurate data below $r \simeq 3.02$.

r	$-\eta^{-1}\dot{E}$	% absorbed
3.02	83(1)	37.7
3.03	39.9(2)	36.3
3.04	23.62(5)	35.1
3.05	15.64(1)	34.1
3.10	4.232549(9)	30.0
3.15	1.9223864(1)	26.9
3.20	1.081977467(7)	24.2
3.30	0.467163243(4)	19.9
3.40	0.25012891219(4)	16.3
3.50	0.1510176014(1)	13.4
3.60	0.09864553444(1)	11.0
3.70	0.06818392468(3)	9.09
3.80	0.0491937318(2)	7.50
3.90	0.03670796106(3)	6.20
4.00	0.02814331203(5)	5.15
4.10	0.02206146488(5)	4.30
4.20	0.01761664969(8)	3.61
4.30	0.01428856144(8)	3.04
4.40	0.01174466751(8)	2.57
4.50	0.00976536837(3)	2.19
4.60	0.00820146283(7)	1.88
4.70	0.00694902541(6)	1.61
4.80	0.00593406093(6)	1.39
4.90	0.00510284885(5)	1.21
5.00	0.00441570494(4)	1.05
5.10	0.00384285426(2)	0.922
5.20	0.00336164181(3)	0.810
5.50	0.00231155387(2)	0.562
5.75	0.00173630600(1)	0.424
6.00	0.00132984067(1)	0.326

TABLE I. Numerical data for the rate of energy loss, $\dot{E} = dE/d\tau$, for a sample of sub-ISCO circular geodesic orbits of radius r . In the second column parenthetical figures show the estimated uncertainty in the last displayed decimals. The third column shows the percentage of energy radiated down the event horizon, $100 \times (dE_{\text{GW}}^-/dt)/(dE_{\text{GW}}/dt)$; all figures shown are significant.

Appendix B: Perturbation modes of the critical solution in the ultrarelativistic limit

Table I displays our numerical results for a sample of orbital radii in the range $3.02 \leq r \leq 6$. We choose to show \dot{E} data from flux calculations, which, we believe, are slightly more accurate. For completeness we also show the flux dE_{GW}^-/dt absorbed by the black hole as a fraction of the total flux radiated. For circular orbits at the ISCO only very little ($\simeq 0.3\%$) of the energy emitted goes down the hole. This fraction, however, becomes very significant for orbits closer to the light-ring, reaching as much as 37.7% at $r = 3.02$. A rough extrapolation gives $\simeq 42\%$ at the light ring itself.

In the independent variable $T := \eta^{-1}T$, with $\hat{\tau}$ defined by (86), (83) becomes

$$\frac{d^2x}{dT^2} - \frac{d \ln \Gamma}{dT} \frac{dx}{dT} - x = 0. \quad (\text{B1})$$

The ultrarelativistic approximations (75) and (88) give $\Gamma \propto T^{\beta/(1-\beta)}$, and so in the ultrarelativistic approximation (B1) becomes

$$\frac{d^2x}{dT^2} - \frac{\beta}{1-\beta} \frac{1}{T} \frac{dx}{dT} - x = 0. \quad (\text{B2})$$

With the substitution

$$x(T) =: T^\nu y(T) \propto \hat{\tau}^{1/2} y(T), \quad \nu := \frac{1}{2(1-\beta)}, \quad (\text{B3})$$

we obtain

$$T^2 \frac{d^2y}{dT^2} + T \frac{dy}{dT} - (T^2 + \nu^2)y = 0, \quad (\text{B4})$$

which is the modified Bessel equation with index ν . Hence two linearly independent perturbation modes of the critical solution are

$$\sqrt{\frac{2\pi}{\nu}} K_\nu(\sqrt{1-\beta} T) \quad \text{and} \quad I_\nu(\sqrt{1-\beta} T)$$

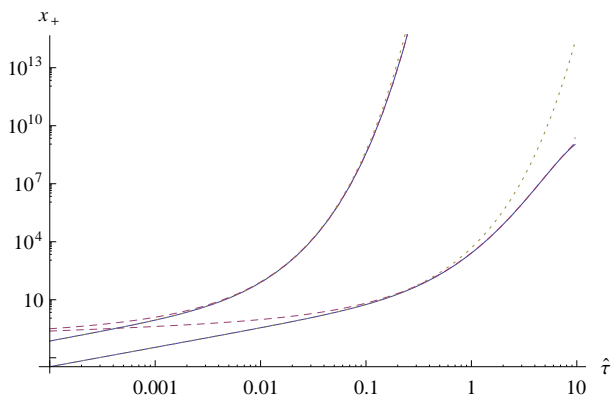


FIG. 12. Log-log plot of the growing perturbation mode $x_+(\hat{\tau})$ for $\eta = 0.1$ (lower curves) and $\eta = 0.01$ (upper curves). The solid lines are numerical solutions started up from (B5) at small $\tau = 0.0001$, the dashed lines are given by the WKB approximation (87) with the *exact* values of $\Gamma(\hat{\tau})$ and $T(\hat{\tau})$, and the dotted lines are the ultrarelativistic (Bessel function) approximation (B5), normalised to agree with the WKB approximation. The power-law growth of both the exact mode and its ultrarelativistic approximation at small τ visible here is in fact linear, as can be shown from (B5). It can be seen that the WKB approximation is good at large $\hat{\tau}$ /small E , and the ultrarelativistic approximation in the other regime. Note that our self-force data are valid only for $\hat{\tau} \gtrsim 0.2$, corresponding to $r > 3.02$. It is clear from the figure that starting the numerical integration with data from the ultrarelativistic approximation at $\hat{\tau} = 0.2$ instead of 0.001 would make little difference for $\eta = 0.1$ and very little difference for $\eta = 0.01$.

-
- [1] V. Cardoso et al., NR/HEP: roadmap for the future, arXiv:1201.5118.
- [2] F. Pretorius and D. Khurana, Black hole mergers and unstable circular orbits, *Class. Quant. Grav.* **24**, S83 (2007).
- [3] K. Martel, Gravitational wave forms from a point particle orbiting a Schwarzschild black hole, *Phys. Rev. D* **69**, 044025 (2004).
- [4] E. Berti *et. al.*, Seminanalytical estimates of scattering thresholds and gravitational radiation in ultrarelativistic black hole encounters, *Phys. Rev. D* **81**, 104048 (2010).
- [5] M. Davis, R. Ruffini, W. H. Press and R. H. Price, Gravitational radiation from a particle falling radially into a schwarzschild black hole, *Phys. Rev. Lett.* **27**, 1466 (1971).
- [6] K. Oohara and T. Nakamura, Gravitational waves from a particle scattered by a schwarzschild black hole. *Prog. Theor. Phys.* **71**, 91 (1984).
- [7] U.Sperhake, V.Cardoso, F.Pretorius, E.Berti, T.Hinderer and N.Yunes, Cross section, final spin and zoom-whirl behaviour in high-energy black hole collisions, *Phys. Rev. Lett.* **103**, 131102 (2009).
- [8] C. Cutler, D. Kennefick and E. Poisson, Gravitational radiation reaction for bound motion around a Schwarzschild black hole, *Phys. Rev. D* **50**, 3816 (1994).
- [9] C. Gundlach and J. M. Martín-García, Critical phenomena in gravitational collapse, *Living Reviews in Relativity*, **2007-5** (2007), last updated in 2010.
- [10] T. Hinderer and E. E. Flanagan, Two-timescale analysis of extreme mass ratio inspirals in Kerr spacetime: Orbital motion, *Phys. Rev. D*, **78**, 064028 (2009).
- [11] L. Barack and N. Sago, Gravitational self force on a particle in circular orbit around a Schwarzschild black hole, *Phys. Rev. D* **75**, 064021 (2007).
- [12] S. Akcay, A Fast Frequency-Domain Algorithm for Gravitational Self-Force: I. Circular Orbits in Schwarzschild Spacetime, *Phys. Rev. D* **83**, 124026 (2011).
- [13] A. Ori and K. S. Thorne, The Transition from inspiral to plunge for a compact body in a circular equatorial orbit around a massive, spinning black hole, *Phys. Rev. D* **62**, 124022 (2000).
- [14] Ref. [7] quotes a maximum fraction of energy radiated of 23%, while its Fig. 2 shows a maximum number of 1.7 orbits; we have divided the former by the latter. For a boost of 2.9, the maximal energy radiated went up to 35%, but the maximal number of orbits is not given.
- [15] M. W. Choptuik and F. Pretorius, Ultra-relativistic particle collisions, *Phys. Rev. Lett.* **104**, 111101 (2010).
- [16] J. Healy, J. Levin and D. Shoemaker, Zoom-whirl orbits in black hole binaries, *Phys. Rev. Lett.* **103**, 131101 (2009).

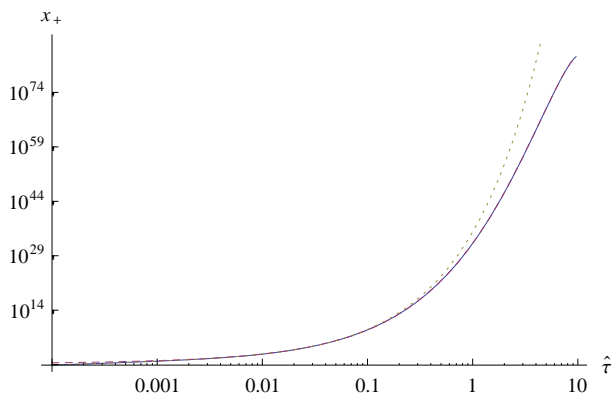


FIG. 13. Log-log plot of the growing perturbation mode $x_+(\hat{\tau})$ for $\eta = 0.01$, showing the full range. The lines are as in Fig. 12. From this and the preceding figure it is clear that the WKB approximation (87) is excellent for $\hat{\tau} \gtrsim 0.2$ for $\eta = 0.1$, and $\hat{\tau} \gtrsim 0.001$ for $\eta = 0.01$. Continuing this trend, the WKB approximation is good from smaller $\hat{\tau}$ (higher energies) for smaller η , and it is always good essentially up to plunge.